Chapter 2
Microresonator Sensors Made in Polymers with Functional Chromophore Dopants

Antao Chen

Abstract The optical properties such as index of refraction and optical absorption of many chromophore-doped polymers are sensitive to the physical and chemical environment to which the polymers are exposed. A variety of microring resonator sensors have been realized with chromophore-doped polymers. Detection sensitivity is further enhanced by optical microresonator structures such as waveguide microring resonator and fiber Bragg gratings. Chromophore-doped polymers also offer some desirable flexibility in device fabrication. Ultraviolet light and electron beam can reduce the index of refraction of the polymer. The photobleaching and electron beam bleaching methods form optical waveguides in a single fabrication step and do not involve solvents or wet chemicals, and can be applied to polymers that are not compatible with other waveguide fabrication techniques.

This chapter provides an overview of the basic principles and designs of such sensors. A chemical sensor to detect trace explosives and a broadband fiber optic electric-field sensor are presented as practical examples. The polymers used for the trace explosive sensor are unpoled and have chromophores randomly orientated in the polymer hosts. The electric field sensor uses a poled polymer with chromophores preferentially aligned through electrical poling, and the microring resonator is directly coupled to the core of optical fiber.

2.1 Introduction

Polymers with specific functionalities can be realized by incorporating various dopants, such as laser dyes, rare earth ions, quantum dots, and functional chromophores into the host polymer. Chromophores are molecules or chemical groups as part of a larger molecule, and they have characteristic absorption bands in the

A. Chen
Applied Physics Laboratory, University of Washington, Seattle, WA 98105, USA
e-mail: antaochen@apl.washington.edu

X. Fan (ed.), *Advanced Photonic Structures for Biological and Chemical Detection*, Integrated Analytical Systems,
DOI 10.1007/978-0-387-98063-8_2,

optical wavelengths, giving them a distinct color. The color of chromophores ranges from red to blue depending on the specific chromophore. Some chromophores have long been used as dyes in the textile industry. If chromophores are randomly oriented in the polymer matrix, the polymer can have strong third-order nonlinear optic (NLO) effect, two-photon absorption and fluorescence, and sensitivity to chemical analytes. Chromophores of electron donor–π electron charge transfer bridge-electron acceptor (D–π–A) structure can have a strong dipole moment and second-order NLO effect. Such chromophores can be preferentially orientated through electrical or optical poling. The poled polymers become electro-optic materials and they have been used for high speed electro-optic (EO) modulation and switching, generation of terahertz signals through optical rectification, and second harmonic generation[1–4]. High electronegative chemicals such as nitroaromatic explosives trinitrotoluene (TNT) and dinitrotoluene (DNT), have shown strong interaction with conjugated charge transfer chromophores and thus change the optical properties of chromophore-doped polymers. This makes such polymers useful in detecting trace explosives[5]. Decomposition of chromophores through exposure to ultraviolet (UV) and energetic electron beam permanently reduces the index of refraction of the polymer. This property can be used to fabricate optical waveguides and microring resonators.

A broad range of optical devices, including wavelength filters, wavelength division multiplexers and demultiplexers, lasers, switches, modulators, dispersion compensators, and polarization rotators can be realized with microring resonators[6–10]. Microring resonators are also a good platform of miniature optical sensors to measure temperature, strain, and stress, and to detect chemical and biological agents[11]. High Q-factor and long photon life-time enhance sensor response. The small size of microring resonators also requires smaller amount of analytes for bio- and chemical sensing. The overall length of conventional optical waveguide devices based on Mach-Zehnder interferometers, directional couplers, Y-branch switches, and multimode interference (MMI) technologies is on the order of a centimeter. In contrast, microring resonator devices have much smaller (several micrometers to a few hundred micrometers) sizes. This unique advantage makes microring resonators ideal for large scale integration to form an array of sensors on a single chip. It also makes them highly suitable for monolithic integration with silicon integrated circuits that interface with the sensors.

Microring resonators have been realized in many different materials, including silicon-on-insulator, GaAs and InP, glass, and polymers[1,6–11]. Polymers offer a number of unique advantages compared to the other materials. Through modern molecular design and organic synthesis, polymers can have tailored optical (index of refraction, birefringence, absorption spectrum), device fabrication processing, and tuning/sensing (electro-optic, thermo-optic, chemo-optic, and photoelastic) properties to meet the requirements of specific applications and device designs. Many fabrication options exist for polymer microring resonators. They can be fabricated by photolithography and reactive ion etching (RIE), imprinting, soft-lithography molding, two-photon polymerization, and electron-beam (e-beam) writing. Polymer optical waveguides can also be fabricated on flexible, curved, and conformal substrates. These advantages allow polymer microring resonators to

have functionality, performance, design, and fabrication flexibilities not available in other materials.

By combining chromophore-doped polymers with optical resonator structures such as waveguide microring resonators and fiber Bragg gratings, a variety of sensors can be made. We have discovered that some polymers containing chromophores of D–π-A structure can have strong interaction with molecules of nitroaromatic compounds such as TNT and DNT[5]. As nitroaromatic compounds represent the major group of high explosives, this new discovery can potentially have applications in homeland security, counter-terrorism, and land mine detection. Unlike electro-optic polymers[12], poling[13] is not necessary for this application, and the chromophores are randomly oriented in the polymer matrix. This naturally avoids possible thermal stability issues associated with poled nonlinear optical polymers. Significant changes in the UV-VIS absorption spectra and indices of refraction have been observed when the polymer is exposed to part-per-billion (ppb) levels of DNT vapor in air. A compact explosive sensor based on microresonators made in chromophore-doped polymers by photobleaching is presented. When a polymer that contains second-order nonlinear optical chromophores is poled and the chromophores are preferentially oriented, the polymer exhibits macroscopic second-order nonlinear optical properties and becomes an electro-optic polymer, and the polymer can be used for electro-optic sensors. The index of refraction of an EO polymer varies with external electric field. A broadband all-dielectric electric field sensor based on electrically poled chromophore-doped polymer[14] is described.

This chapter covers the recent progress in optical sensors based on microresonators made with chromophore-doped polymers. The chapter begins with basic theory of optical microring resonator sensors and a description of a simple approach that has been found effective in optimizing the design of microring resonators. Photobleaching and electron-beam bleaching fabrication of microring resonators with submicrometer feature size are described. These techniques are unique to chromophore-doped polymers. Finally two practical examples, a trace explosive sensor using an unpoled polymer and a broadband electric field sensor using a poled polymer will be discussed in detail.

2.2 Microring Resonator Theory and a Design Method

2.2.1 Basic Theory of Microring Resonators

Basic microring resonators consist of a ring waveguide as a resonant cavity and one or two bus waveguides, which are coupled to the ring waveguide and provide input and output ports for the device. When the round-trip phase shift of the ring waveguide is equal to multiples of 2π, circulating lights of different cycles in the ring interfere constructively with each other and build up resonance modes. As resonance occurs, light from the input port is trapped in the ring and the optical power of these resonance wavelengths are minimized at the through port, as shown in Fig. 2.1a, b.

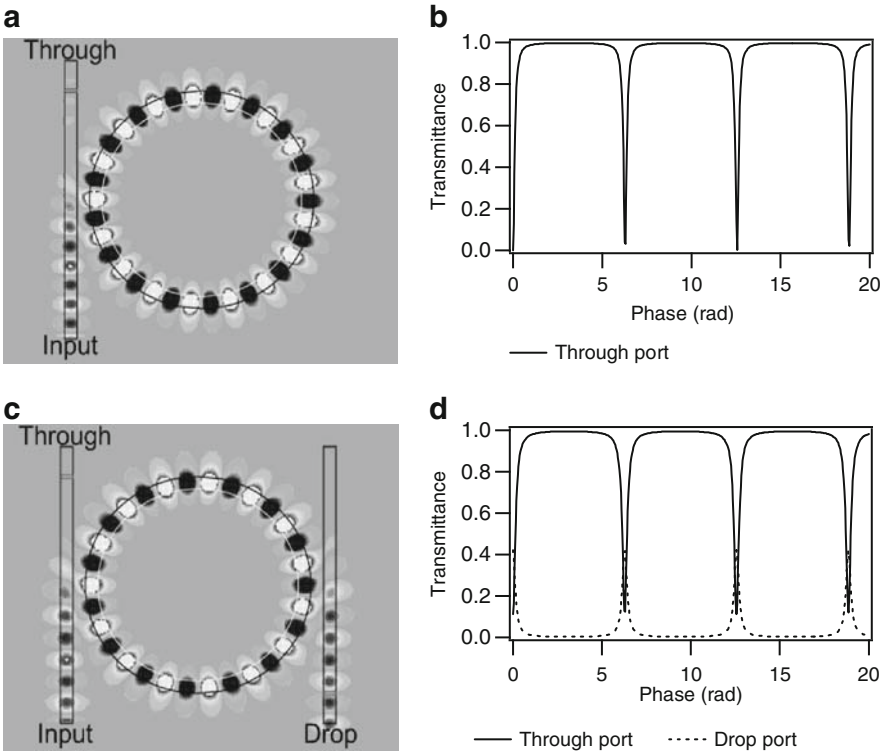

Fig. 2.1 Basic microring resonator structures and their output characteristics. (**a**) One ring resonator and one bus waveguide and (**b**) the corresponding resonance spectrum at the through port. (**c**) One ring resonator and two bus waveguides and (**d**) the corresponding resonance spectrum at the through port and drop port. Reprinted from Ref. 15 with permission. © 2008 Institute of Electrical and Electronics Engineers

If there is a second bus waveguide coupled to the ring, the light trapped in the ring will be coupled out to the second bus waveguide and resonance peaks will be present in the spectrum at the drop port (Fig. 2.1c, d). Because the round-trip phase shift of the ring waveguide is a function of both wavelength and the index of refraction of the waveguide material, the output power of the microring resonator varies with both wavelength and index of refraction. Resonance in the wavelength domain is the basis of channel filters and lasers, and the resonance shift due to the change of the index of refraction, which can be induced by external electric field or chemical analytes, forms the basis of optical switches, modulators, and sensors.

2.2.2 Sensitivity of Microring Resonator Sensors

The sensitivity in detecting the index of refraction change can be estimated using the maximum slope of the resonance and a minimum detectable change in the

power at the optical output end. The minimum detectable change is usually limited by the noise equivalent power of the optical detector. For slow-varying signals such as outputs from chemical, biological, and temperature sensors, a relative intensity change of 0.2% is generally accepted as a detection limit criterion for optical sensors such as surface plasmon resonance (SPR) sensors[16–18].

The sensors are intended to be built with microresonators of high extinction for a large dynamic range; in such case the normalized optical power at the output of the fiber can be express as[19]

$$I_{\text{out}} = \frac{2\alpha^2(1-\cos(\theta))}{1+\alpha^4-2\alpha^2\cos(\theta)}, \tag{2.1}$$

where α is the round-trip loss factor ($0 \leq \alpha \leq 1$). θ is the round-trip phase shift of the resonator

$$\theta = \frac{2\pi^2 n_{\text{eff}} d}{\lambda_0}, \tag{2.2}$$

where n_{eff} is the effective index of the resonant mode, d is the diameter of the resonator, and λ_0 is the free-space wavelength.

Using a free-space wavelength of 1.55 μm (at which fixed and tunable wavelength telecom diode lasers are available at relatively low cost, and also in the low loss window of optical fiber), an effective index of refraction of 1.45, and a ring diameter of 50 μm, the full width half maximum $\Delta\theta_{\text{FWHM}}$ (with coupling taken into account) can be calculated numerically using (2.1). From $\Delta\theta_{\text{FWHM}}$ the loaded Q factor and the finess as a function of the total optical loss of the resonator are calculated and plotted in Fig. 2.2a. The Q factor is the ratio of the resonant wavelength over the wavelength full width half maximum of the resonance. The finess is the ratio of the separation of adjacent resonant wavelengths over the wavelength full width half maximum. Finess is an important factor when building sensor arrays with large number of microresonators on the same bus waveguide. Figure 2.2a shows that for a typical waveguide loss (due to absorption, surface scattering, and bending) of 1 dB/cm, a loaded Q of 10^5 can be reached. A Q of 10^6 requires a waveguide loss of 0.1 dB/cm. This level of low loss is challenging, yet still possible since optical waveguides with a low loss of 0.03 dB/cm (at 1.55 μm. 0.01 dB/cm at 830 nm, including the absorption and scattering losses) have been demonstrated previously[20–22].

The steepest slope can be found from the derivative $dI_{\text{out}}/d\theta$. Using the steepest slope and the criterion of 0.2% relative change of output intensity[16–18], the minimum detectable refractive index changes at various Q are calculated and given in Fig. 2.2b. With a Q factor of 10^6 (total loss of 0.1 dB/cm), an index of refraction change as small as 1.75×10^{-9} RIU (refractive index units) can be detectable, which is about 100 times better than that of typical SPR sensors. If the total loss could be kept below 0.04 dB/cm (based on the 0.03 dB/cm loss demonstrated from straight waveguides[20,21] plus 0.01 dB/cm for waveguide bending

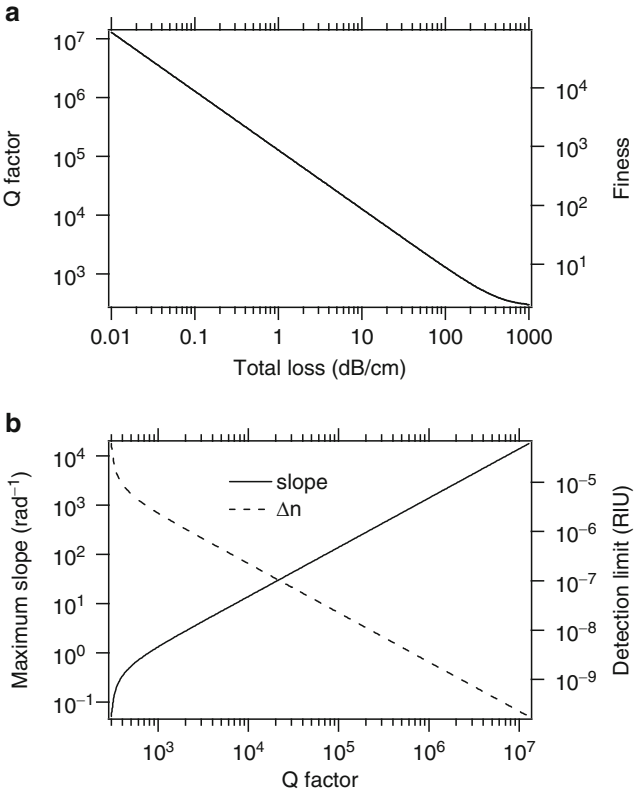

Fig. 2.2 (**a**) The loaded Q and finess of a 50 μm diameter ring resonator as a function of the total waveguide loss. The coupling loss is taken into account in the calculation (critical coupling is assumed). The total waveguide loss includes material absorption loss, waveguide bending loss, and scattering loss due to surface roughness and index inhomogeneity. (**b**) Maximum slope in rad^{-1} and sensitivity (minimum detectable change in refractive index) as functions of Q. The data are calculated using the 0.2% intensity variation criterion, a 50 μm ring diameter, and 1.55 μm wavelength

loss), the theoretical detection limit would be 7×10^{-10} RIU. For a given microring resonator, sensitivity scales with $1/\lambda_0^2$. Using a shorter wavelength could also significantly improve the sensitivity. As a side benefit of using shorter wavelengths, the optical losses of polymers are lower at shorter wavelengths than at telecom wavelengths. Polymer waveguides with loss as low as 0.01 dB/cm has been reported at the wavelength of 830 nm[22].

The above estimation is based on slow varying quasi-DC signals. For fast oscillating AC signals such as acoustic, ultrasound, and radio frequency (RF) electromagnetic waves, advanced detection techniques (low noise amplification, filtering, heterodyne, phase locked loop, etc.) developed in these technical areas and in optical telecom could be used to reach sensitivities much higher than the sensitivity based on the 0.2% DC detection criteria[23].

For an RF electric field sensor, bandwidth (speed) is another important requirement. The speed of a resonator is determined by the cavity ring down time $\tau = Q\lambda/c$. As in any devices using resonating structures, a trade off between sensitivity (which increases with Q) and speed (which decreases when Q increases) has to be made. At the wavelength of 1.55 μm, Q factors of 10^4 and 10^6 translates to a sensor bandwidths of 20 GHz and 200 MHz, respectively.

2.2.3 A Simplified Approach to Designing Microring Resonators

Q-factor and extinction ratio are two most important figures of merit of resonators. The Q is mainly affected by the scattering and bending loss of the ring waveguide, and the maximum extinction ratio is achieved when the critical coupling condition[19] is met. To vigorously model the complete microring resonator device the finite-difference time-domain (FDTD) algorithm needs to be used. FDTD solves the Maxwell's equations without making major approximations or assumptions to compromise the accuracy. However, FDTD algorithm is very computationally intensive and cluster computers are normally required to realistically model a microring resonator. The outputs from FDTD codes also require a great deal of postprocessing to extract device performance information such as resonant wavelengths, the Q-factor, the resonance extinction ratio, and the free spectral range (FSR).

A time-saving and much simpler approach is to divide the microring resonator into its building blocks and to consider the microring resonator as an optical circuit made of directional couplers and curved waveguides, as illustrated in Fig. 2.3. Beam propagation method (BPM) algorithm can separately calculate the coupling

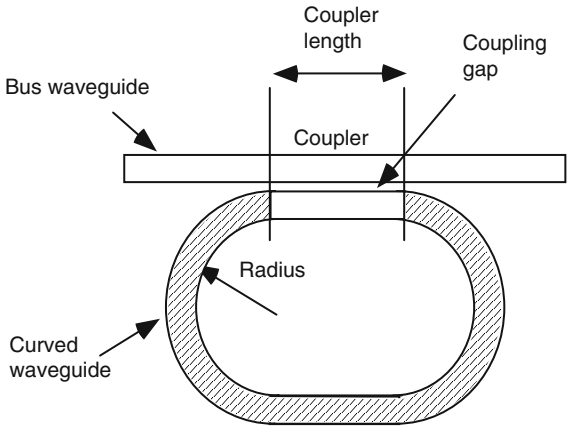

Fig. 2.3 By regarding a basic microring resonator as an optical circuit composed of a directional coupler and a curved waveguide (the cross hatched section), the characteristics of the microring resonator can be analyzed using simpler BPM code and transfer matrices instead of computation intensive FDTD simulation. Reprinted from Ref. 15 with permission. © 2008 Institute of Electrical and Electronics Engineers

ratio of directional couplers, the propagation constant, and loss of curved waveguide with satisfactory accuracy. A BPM code is much faster and requires much less computer memory than an FDTD code and the BPM simulation can be easily carried out on a standard personal computer. The results from the BPM simulation are then used to construct transfer matrices [24,25] that represent couplers and the ring waveguide. Transmission properties of every specified output port can be obtained by using the transfer matrices. For example, the calculated round-trip loss factor $|\alpha|^2$ for various index contrast and radius of curvature and the coupler attenuation $|t|^2$ vs. coupler length and gap, are plotted in Fig. 2.4a, b, respectively. From Fig. 2.4a one can find the possible combinations of index contrast and radius of curvature to maximize the $|\alpha|^2$ and Q. The figure clearly shows that smaller radius requires larger index contrast. For any given index contrast, there exists a peak of $|\alpha|^2$ and an optimal radius. Below the optimal radius the bending loss increases sharply, and above the optimal radius the perimeter of the ring increases and the round trip loss increases with it. After the peak $|\alpha|^2$ is determined the next step is to match $|t|^2$ with $|\alpha|^2$ using Fig. 2.4b to find the possible combinations of coupler length and gap to meet the critical coupling condition for maximum extinction ratio. Wider (>1 μm) gap or zero gap (MMI) couplers are often preferable because they have relatively large critical feature size and are easier to fabricate. By using this simple procedure one can quickly determine the approximate values of the key design parameters. From there an optimal design can be found by experimenting a number of design variations around these values.

2.3 Waveguide Fabrication Techniques Unique to Chromophore-Doped Polymers

2.3.1 Photobleaching

Traditional methods to fabricate polymer waveguide devices is patterning a photoresist etch mask on the polymer film, and then using RIE to transfer the photoresist pattern to polymer film, and finally removing the remaining photoresist on the waveguide. It is a process of multiple fabrication steps. The solvent in the photoresist often reduces the surface quality of the polymer and in some cases can dissolve the polymer and destroy the film. In these cases a method to fabricate polymer waveguides without using solvent or wet chemistry is highly desirable. For both poled and unpoled chromophore-doped polymers, optical waveguide can be patterned in a single step using ultraviolet light or electron-beam.

Conjugated charge transfer chromophores are more polarizable than the polymer host and polymers doped with chromophores have index of refraction higher than that of the host polymer alone. High-energy ultraviolet photons can break chemical bonds and destroy the conjugated-charge transfer system of the organic chromophores. Consequently, the index of refraction of the chromophore-doped optical polymer is reduced. Photobleaching has been used to make single mode channel

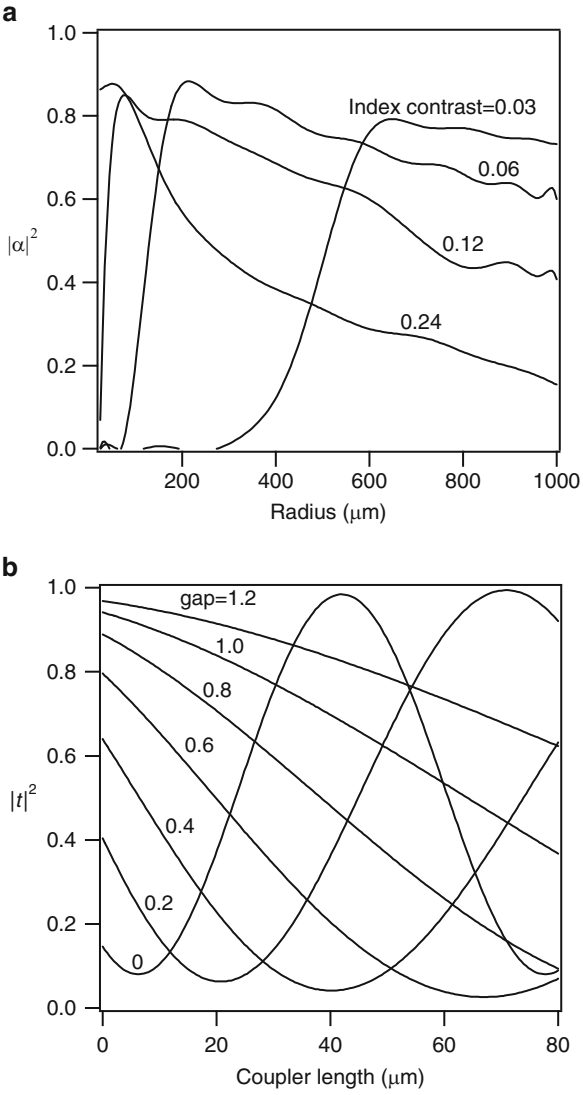

Fig. 2.4 BPM simulation results for polymer microring resonators: (**a**) Round trip attenuation vs. the core-cladding index contrast and radius of curvature. (**b**) Coupling induced attenuation vs. the length and gap of the coupler. The width and height of the waveguide is 2 μm. The wavelength used in the calculations is 1.55 μm. Reprinted from Ref. 15 with permission. © 2008 Institute of Electrical and Electronics Engineers

waveguides[26] and to perform postfabrication trimming of polymer waveguide devices[27]. Photobleaching through a photomask forms optical waveguides in a single step. It not only simplifies the device fabrication, but also reduces the sources of error from multiple fabrication steps. Photobleaching is a dry process and does not use solvents and wet chemicals.

The effectiveness of photobleaching in fabricating microring resonators[28] has been demonstrated in an amorphous polycarbonate (APC) doped with 25 wt.% of AJL8 chromophore (AJL8/APC). The chemical structure of AJL8 is given in Fig. 2.5. Figure 2.6 shows the change of the absorption spectra and refractive index of the AJL8/APC polymer after various degrees of exposure to UV light of 365 nm wavelength, indicating a permanent change of the material. In Fig. 2.6a, the absorption peak at 714 nm is the characteristic peak of the conjugated charge transfer system of the π-orbital electrons of the chromphore. The disappearance of the characteristic peak clearly indicates an irreversible photochemical decomposition of the chromophores. A decrease of refractive index as large as 0.08 RIU was observed. According to Fig. 2.4a, such index contrast is sufficient to make microring resonators of radius as small as 200 μm.

Photobleaching also reduces the thickness of the EO polymer by 80 nm, or 6%. The original thickness of the polymer film was 1.3 μm. Atomic force microscopy (AFM) picture (Fig. 2.7) of a photobleached waveguide shows that the corresponding cross-section profile matches the near-field diffraction pattern of the opaque line on the photomask. The decrease of thickness in the photobleached area is because some photodecomposition products are gaseous and diffuse out of the polymer thin film, and the volume of the polymer is reduced. AFM scan indicates that the photobleached region has the same level of surface smoothness as the unbleached region. Single mode waveguides were obtained for waveguides of width smaller than 6 μm. Waveguide losses were measured by cutback method. The propagation loss was found to be 2.3 dB/cm and 2.0 dB/cm for the horizontal (TE) and vertical (TM) polarizations, respectively. These loss values are similar to the losses of the ridge waveguides made from the same material by photolithography and RIE. Coupling loss between the fiber and the waveguide was 4 dB, which is also typical for the polymer waveguides with same mode size.

Based on the measurement and BPM simulation results, microring resonators were designed using the method described in the previous section. The ring waveguides are race track shaped and have 80 μm coupling length and 200 μm radius. The width of the waveguide is 4 μm. The AJL8/APC was spin cast from solution to form a film about 1 μm in thickness on a silicon wafer with 4 μm silicon dioxide. The silicon dioxide functions as a lower cladding for the polymer waveguides. Devices with coupling gaps ranging from 0.6 to 1.2 μm were fabricated and tested. A photomask made by electron-beam lithography was used to define the waveguides. The highest extinction ratio was obtained from resonators with a coupling gap of 1.1 μm. The resonance extinction ratio is 16 dB for TE and 7 dB for TM polarization, as shown in Fig. 2.8. The FSR between adjacent resonances was approximately 1.08 nm, which is in good agreement with the theoretical calculation. The Q factor of the resonators was obtained by fitting the theory to the experimental data and the Q was found to be in the range of 6,500–8,100. The insertion loss at the peak transmission was 8.7 dB, which is mainly due to the fiber-to-waveguide coupling at the input and output ports of the device.

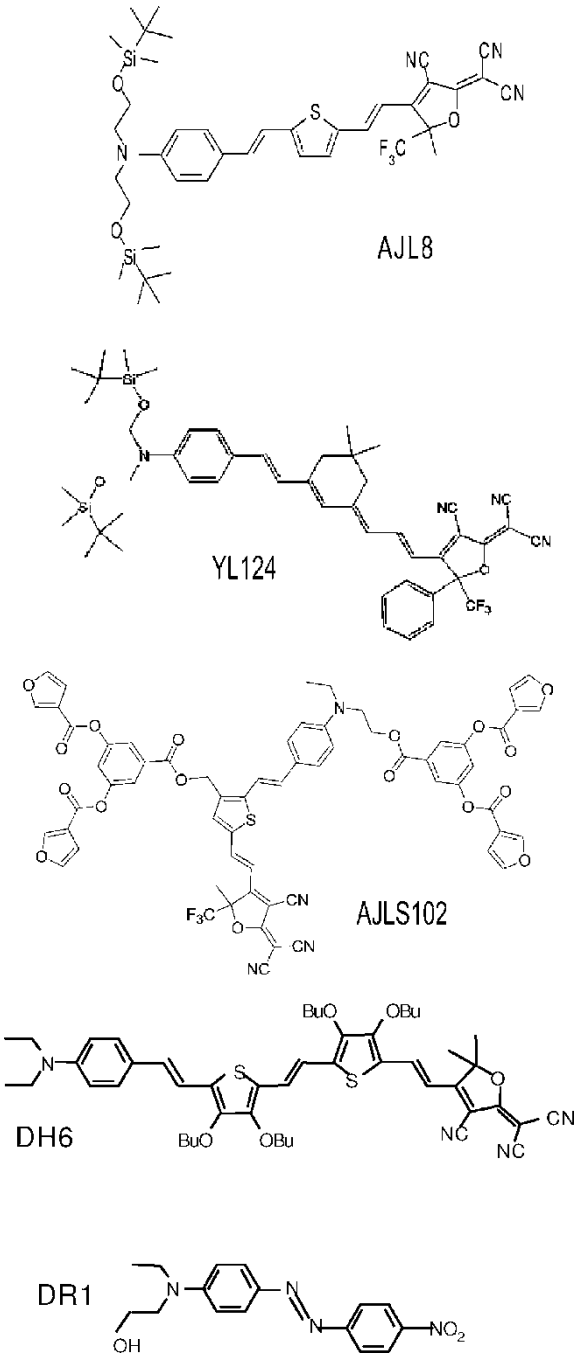

Fig. 2.5 Chemical structures of the chromophores used in this work. Reprinted from Ref. 15 with permission. © 2008 Institute of Electrical and Electronics Engineers

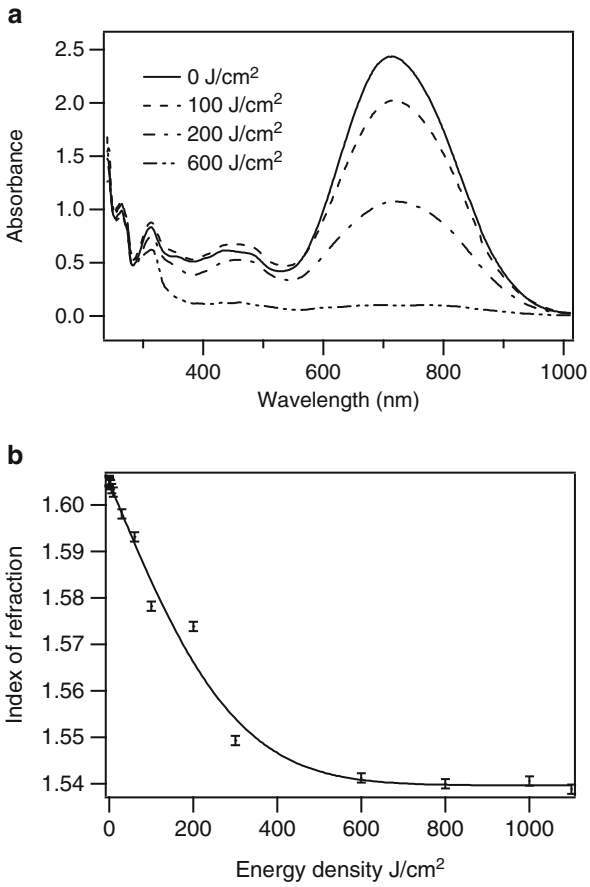

Fig. 2.6 The characteristic absorption peak disappears (**a**) and the refractive index decreases (**b**) as the photobleaching energy density increases. The refractive index was measured at the wavelength of 1.55 μm. Reprinted from Ref. 15 with permission. © 2008 Institute of Electrical and Electronics Engineers

2.3.2 Electron-Beam Bleaching

The resolution limit of photobleaching using ultraviolet light is about 1 μm. Sometimes the optimal design of microring resonator calls for a coupling gap much smaller than 1 μm. For instance, in order to achieve a large FSR the round-trip optical path needs to be minimized and therefore the coupler needs to have smaller gap in order to make the coupler shorter. Couplers with submicron coupling gaps can be made by electron-beam bleaching. Electron beam irradiation induced a refractive index decrease of about 0.06 RIU in polymethyl methacrylate (PMMA) polymer doped with YL124 chromophores[29] (Fig. 2.5). The degree of index change is similar to what is observed with photobleaching. Similarly, a decrease in the

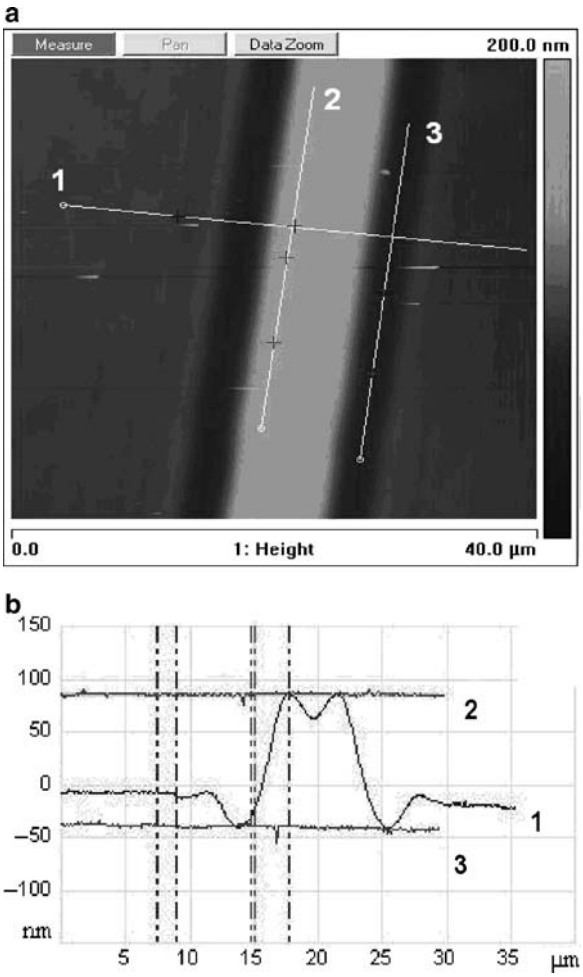

Fig. 2.7 The topographic view of a photobleached waveguide using atomic force microscopy (**a**), and the height profile along three scan lines (**b**). Reprinted from Ref. 15 with permission. © 2008 Institute of Electrical and Electronics Engineers

thickness of the polymer film after e-beam bleaching is also observed. Electron beam provides nanometer scale resolution, and microring resonators with critical feature size of 100–200 nm are readily achievable. E-beam bleaching can be carried out by a standard scanning electron microscope (SEM) with a pattern generator. Without the need of expensive high resolution photomasks, different designs of microring resonator devices can be generated easily with electron beam bleaching. This is especially effective for fast prototyping and design optimization. As with the photobleaching, electron beam bleaching is a single-step process and does not use wet chemicals. The waveguides are formed by exposing a strip of 20–50 µm wide on each side of the waveguide to create low index clad for lateral confinement,

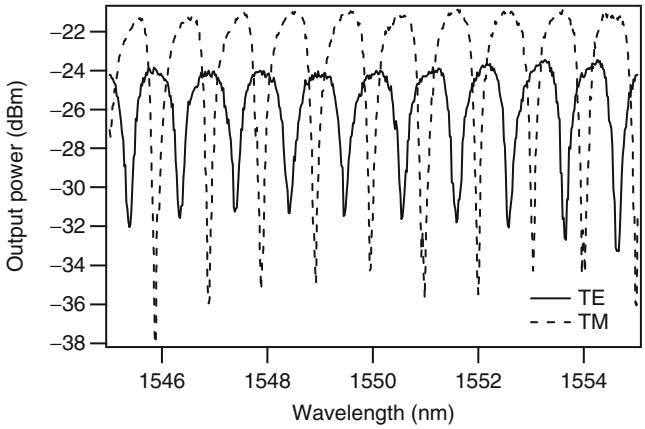

Fig. 2.8 Transmission spectrum of a microring resonator with 1.1 μm coupling gap. Reprinted from Ref. 15 with permission. © 2008 Institute of Electrical and Electronics Engineers

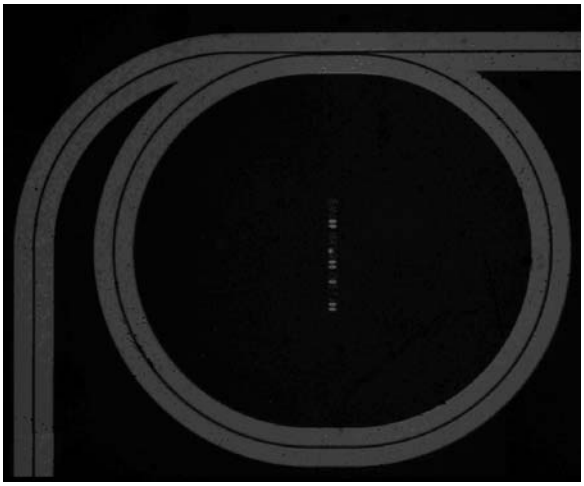

Fig. 2.9 A microscope image of a microring resonators fabricated with the electron beam bleaching method. The lighter areas in the image are bleached by electron beam. Reprinted from Ref. 15 with permission. © 2008 Institute of Electrical and Electronics Engineers

as shown in Fig. 2.9. It is found that it is not necessary to coat the polymer thin film with metal or conductive polymer during the e-beam exposure. This is different from SEM imaging of polymer samples, in which a conductive coating is usually required to prevent surface charging.

For a microring resonator with a waveguide width of 5 μm and coupling gap of 200 nm, a resonance extinction ratio of 12 dB for TE polarization and 9 dB for TM polarization has been achieved, as shown in Fig. 2.10. The ring resonator had a race track shape with circular sections of 500 μm radius and straight coupling section of 100 μm in length. The width of the two exposed strips is about 50 μm.

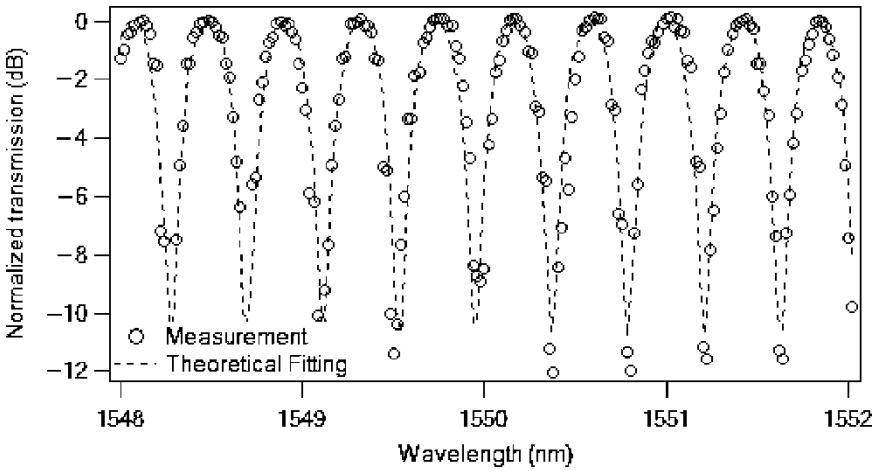

Fig. 2.10 Normalized transmission spectrum of a microring resonator made by e-beam bleaching. The input light is TE polarized. Reprinted from Ref. 15 with permission. © 2008 Institute of Electrical and Electronics Engineers

The polymer used is PMMA doped with YL124 chromophore at 20 wt% and the thickness of the polymer film is 2 μm. The film was spin coated on silicon substrate with 5 μm of thermal oxide as lower cladding. The microring resonator was patterned with a FEI Sirion SEM equipped with a nanometer pattern generation system. Accelerating voltage of 30 kV and beam current of 5 nA were used to reduce the e-beam writing time. For this polymer, the change of index saturates at e-beam dose above 500 μC/cm^2 and the dose of electron beam exposure used to pattern the microring resonator was 700 μC/cm^2.

2.4 Change of Linear Optical Properties Caused by Nitroaromatic Explosives

Recently we have observed that the trace vapors of electro-negative nitroaromatic explosives such as TNT and DNT cause significant changes in the linear optical properties, i.e., index of refraction and absorption spectrum, of certain chromophore-doped polymer thin films. Figure 2.11 shows the UV-VIS-NIR absorption spectra of a thin film of polymethylmethacrylate (PMMA) doped with chromophore DH6[30] (shown in Fig. 2.5) at 20 wt.% after various duration of exposure to DNT vapor in the air. The polymer films were spin coated from solution on glass slides, and dried overnight in vacuum at 60–70°C. The thickness of the film is 1 μm. The film is not electrically poled and the chromophores are randomly orientated in the matrix of the PMMA host. The main absorption peak originally at 630 nm shows a red shift as large as 70 nm and a reduced peak absorbance from 1.53 to 0.3 after

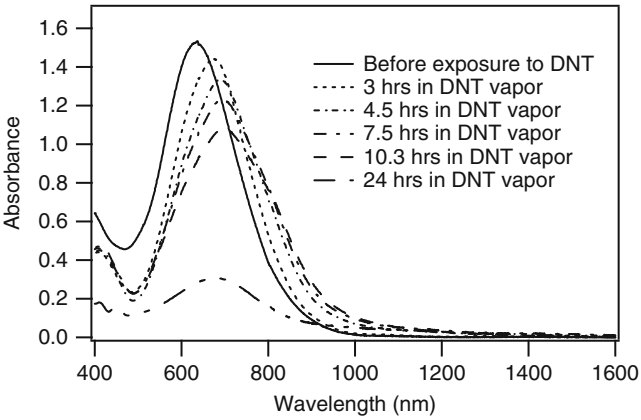

Fig. 2.11 Absorption spectrum of a DH6/PMMA thin film after it is exposed to DNT vapor at 65°C for various periods of time. The peak at about 630 nm is the characteristic absorption peak of the chromophore. Reprinted from Ref. 33 with permission. © 2008 American Chemical Society

the film is exposed to saturated DNT vapor in air at 65°C for 24 h. Similar changes have also been observed at room temperature although the same degree of change took place about ten times more slowly. There is also a noticeable change of color of the film after it is exposed to DNT vapor. The color of the polymer film changes from dark blue to light purple. The changes in the absorption spectrum and the corresponding color changes were observed in a number of host polymers doped at various levels with several different chromophores (DH6[30], AJL8[31], DR1[32]) of the D–π-A structure shown in Fig. 2.5. The type of host polymer (PMMA, APC, and bisphenol-A-polycarbonate) and solvent (chloroform and cyclopentanone) used to make the polymer solutions have only minor effect on the polymer thin film's response to DNT.

Accompanying the change in the absorption spectrum is a change in the index of refraction. Chromophores of D–π-A structure are highly polarizable and contribute to the index of refraction of the polymer. The polarizability, and therefore the index of refraction, can be affected by the electric field acting on the chromophore due to the local environment. The local electric field environment can, in turn, be affected by nitroaromatic explosive molecules that are highly electronegative and polar. To study the sensitivity and specificity of the polymer as trace explosive sensor materials, similarly prepared thin films of 20 wt.% AJL8 chromophore in APC host were, respectively, exposed to saturated vapors of DNT as well as other chemicals that are a common cause of false positives of explosives sensors. These chemicals include pollutants commonly found in the environment, e.g., salts, chemical fertilizers, and detergents. The thin film samples were individually sealed in separate containers with each of these chemicals, and thereby exposed to, at most, a saturated vapor concentration of these chemicals at ambient condition. The concentration of saturated DNT vapor in air at room temperature is known to be 100–120 parts-per-billion[34]. The index of refraction of these thin film samples was

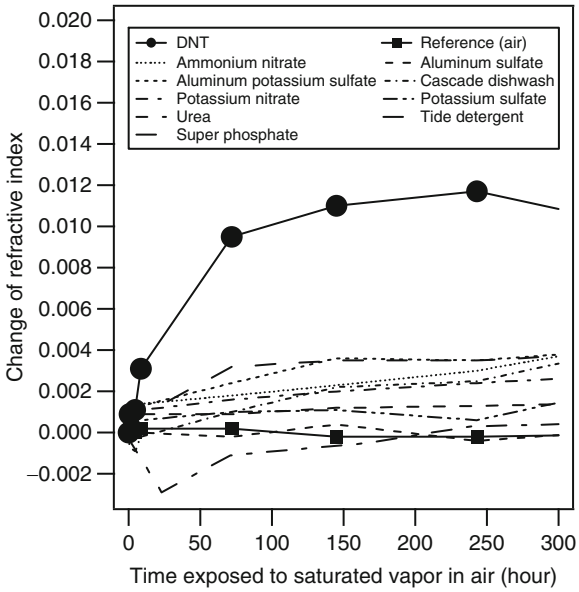

Fig. 2.12 The change of the index of refraction due to DNT is much larger than the change due to other chemicals found in the environment as pollutants. The polymer is 20 wt.% AJL8 chromophore in APC. Reprinted from Ref. 33 with permission. © 2008 American Chemical Society

measured at the wavelength of 1,550 nm with a prism coupler (Metricon 2010) after various time periods of the exposure to the chemical vapors. Figure 2.12 shows the index of refraction change of these samples over time. These results indicate that this polymer has good specificity to DNT. The maximum refractive index change of this polymer is 0.012 RIU at 100–120 ppb of DNT vapor concentration at room temperature. Considering that the index of refraction can be measured with a sensitivity of 10^{-7} RIU with well-engineered polymer microring resonators[11], a detection limit based on the index change of this polymer of 1 parts-per-trillion is practical. In general, the change in the index of refraction can be measured more accurately than the change in the absorption spectrum, for example, using microring resonators and fiber Bragg gratings. Therefore, sensors based on the refractive index change could be more sensitive than the sensors based on the absorption spectrum change.

The details of how nitroaromatic explosive molecules interact with the chromophores in the polymer matrix requires further study. Initial observations suggest that because nitroaromatic explosive molecules are highly electron-deficient, that chromophores have an electron-rich donor and bridge, and that both nitroaromatic explosives and chromophores are highly polar, explosive molecules and chromophores have a strong tendency to interact with each other. The interaction between explosives and the polymer takes place in two steps. In the initial step nitroaromatic explosive molecules create a more polar environment around the chromophores. The increased polar environment produces a solvatochromic red-shift of the

absorption peak of chromophores, and a relatively small (on the order of 10^{-3} RIU) change in the index of refraction of the polymer. The effects of this step are reversible and the polymer recovers after it is removed from explosive vapors. If the polymer continues to be exposed to explosive vapors, more explosive molecules diffuse into the polymer, and the interaction enters the next step. Chromophores and explosive molecules start to form charge transfer complexes. Explosive molecules start to alter the band structure and disrupt the charge transfer bands of the chromophore, and the absorption peak begins to diminish, accompanied by a large (on the order of 10^{-2} RIU) change in the index of refraction. Both interactions are evident in Fig. 2.11, with an initial red-shift of the absorption peak followed by the subsequent reduction of the height of the absorption peak. The strong interaction of the second step was only observed in solid thin films, and the spectral change does not recover even after the film is subsequently baked at temperatures above 100°C for several days, indicating that the interaction between the chromophores and explosives is stronger than the thermal energy. Simply adding nitroaromatic explosives to the chromophore solution does not cause noticeable change of the chromophore absorption peak of the solution. Furthermore, if the polymer film that undergoes the absorption peak reduction after long exposure to explosives is redissolved in the solvent, the absorption spectrum returns to its original shape, as shown in Fig. 2.13. This recovery suggests that the interactions between chromophore and nitroaromatic explosives are physical in nature, rather than a chemical reaction. When the film is redissolved in the solvent, solvent molecules also interact with the chromophores and compete with explosives molecules. Since solvent

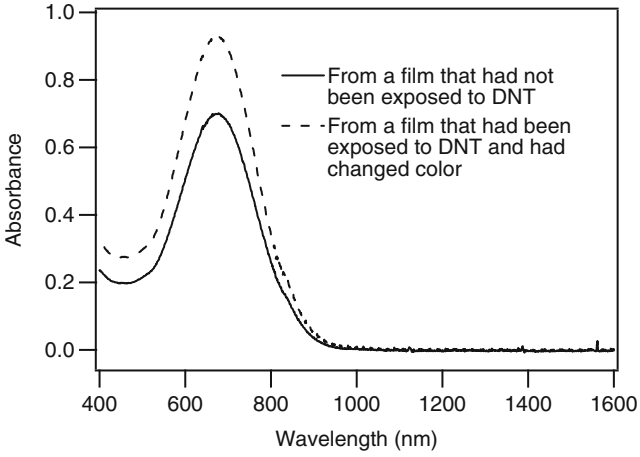

Fig. 2.13 Comparison of the absorption spectra of two DH6/PMMA thin films redissolved in cyclopentanone. One is a pristine film without being exposed to DNT and the other is a film that has been exposed to DNT and has changed color. After they are redissolved in solvent, the absorption spectra of both samples have the same peak wavelength and shape. The difference in the height of the peak is due to the difference in the concentration of the two polymer solutions, and is not important in the comparison. Reprinted from Ref. 33 with permission. © 2008 American Chemical Society

molecules in the polymer solution far outnumber explosive molecules, the solvent separates the explosive molecules from the chromophores.

For the AJL8/APC polymer, saturation was not achieved until 250 h of exposure to the DNT vapor. However, the sensing polymer produces a detectable amount of refractive index change within a few minutes of exposure to DNT vapor of 100 ppb concentration. The response rate is thought to be limited by the diffusion of DNT molecules into the polymer. In the initial experiments reported here PMMA and polycarbonate were used as the host polymers. These polymers are relatively less permeable to DNT. The response rate is expected to improve if a more permeable polymer host is used.

2.5 Poling and Electro-Optical Polymer

The electro-optic property of EO polymers comes from the NLO chromophores. When these chromophores are preferentially aligned to break the centrosymmetry of the material, the molecular level microscopic NLO effect of the molecules translates to the macroscopic second-order NLO effect of the polymer material. The poled material exhibits a strong macroscopic electro-optic effect.

An external electric field induces a change in the dipole moment known as polarization. However, the induced dipole moment has a saturation behavior which makes the polarization deviate for the linear response to the external E-field, and the total polarization p of the chromophore in an external electric field can be written as

$$p_i = \alpha_{ij}E_j + \beta_{ijk}E_jE_k + \gamma_{ijkl}E_jE_kE_l + \ldots, \tag{2.3}$$

where α_{ij} is the linear polarizability, β_{ijk} is the first hyperpolarizability, and γ_{ijkl} is the second hyperpolarizability. $E_{i,j,k}$ are electric field components in the molecular coordinate system. The β term gives rise to the second-order NLO effect.

A polymer system with NLO chromophores randomly oriented does not allow even order nonlinear optical effect due to the central symmetry of the system. In EO polymers, these individual chromophores need to be aligned toward one direction by poling[35–37] to break the central symmetry of the polymer system. Poling is usually done by applying a strong DC field to the polymer. The poling field exerts a torque on these dipolar chromophores and rotates them so that they become preferentially orientated in the direction of poling field. The EO tensor of an EO polymer poled in the z direction is given by

$$\begin{pmatrix} 0 & 0 & r_{13} \\ 0 & 0 & r_{13} \\ 0 & 0 & r_{33} \\ 0 & r_{13} & 0 \\ r_{13} & 0 & 0 \\ 0 & 0 & 0 \end{pmatrix}. \tag{2.4}$$

r_{33} is typically several times greater than r_{13}. EO polymers in general have r_{33} in the range of 10–500 pm/V[38]. When an electric field E_z is applied to an EO polymer and the field is along the poling axis z, the refractive index of the EO polymer will change due to the linear electro-optic effect (the Pockels effect). The changes of ordinary index n_o (for light polarized perpendicular to the poling axis) and extraordinary index n_e are given by

$$\Delta n_o = -\frac{1}{2} n_o^3 r_{13} E_z \tag{2.5}$$

and

$$\Delta n_e = -\frac{1}{2} n_e^3 r_{33} E_z. \tag{2.6}$$

2.6 Microresonator Trace Explosive Sensor

The sensor is a microring resonator fabricated in the polymer thin film of 25 wt.% AJL8/APC polymer fabricated with photobleaching method. The width of the waveguide is 4 μm and the ring is in a race track shape. The straight sections are 80 μm long and the curved sections have a radius of 200 μm. The coupling gap is 1.1 μm. When the sensor is exposed to saturated DNT vapor at room temperature, a resonance shift toward longer wavelength was observed (Fig. 2.14a). The shift of resonance indicates an increase in the refractive index of the polymer consistent with the thin-film refractive index measurement results. After 1 h of exposure the shift was 1.2 nm and the maximum effect has not yet been reached. After removing the sensor from the DNT atmosphere, the sensor properties returned to their initial conditions (Fig. 2.14b). The sensor response was determined by measuring the wavelength of a resonance mode using an optical spectrum analyzer. A typical optical spectrum analyzer can measure the resonant wavelength to an accuracy of 0.05 nm. This accuracy corresponds to an accuracy of 0.00005 RIU for index of refraction measurements, and a sensitivity of ~5 ppb. Polymer microring resonators with optimized design and fabrication conditions and more accurate measurement instrument have demonstrated[11] an index of refraction measurement accuracy of 10^{-7} RIU, which corresponds to a detection sensitivity of a few parts-per-trillion (ppt).

In addition to polymer waveguide microring resonators, we also made trace explosives sensors by incorporating a fiber Bragg grating with the same polymer. The fabrication begins on a commercial fiber Bragg grating. The grating section of the fiber is first etched with hydrofluoric acid and the diameter of the fiber is reduced from 125 μm to about 30 μm. This allows the evanescent tail of the fiber

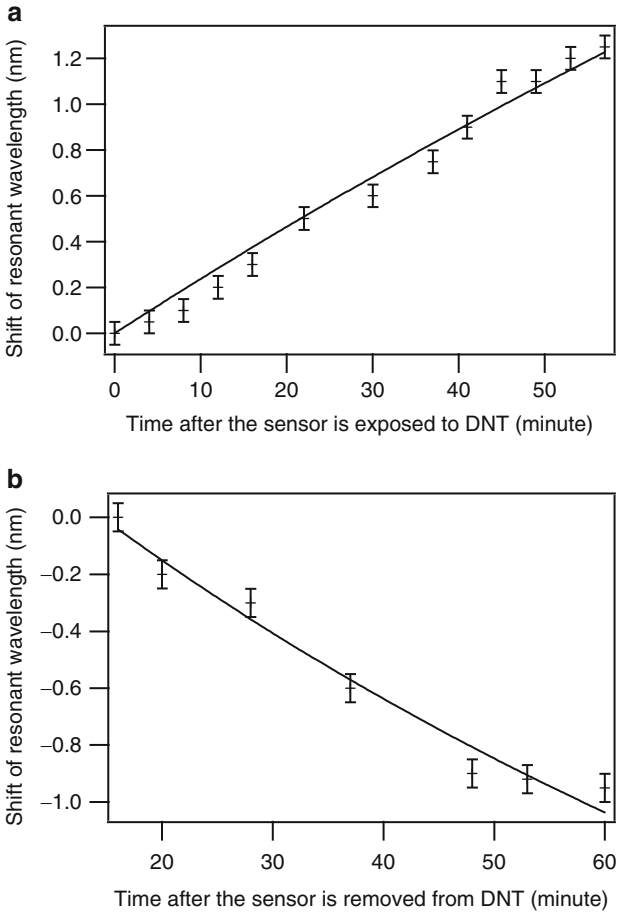

Fig. 2.14 The output of the sensor when it is exposed to (**a**) and removed from (**b**) saturated DNT vapor at room temperature. Reprinted from Ref. 33 with permission. © 2008 American Chemical Society

mode to extend into the polymer coating to probe the change of the refractive index of the polymer. The polymer is coated on the etched area of the fiber by dipping the fiber in the polymer solution and letting the coating dry with the fiber held in the vertical position. The thickness of the coating is about 1 μm. The change in the index of refraction of the polymer coating shifts the resonance of the fiber, as shown in Fig. 2.15. After the sensor fiber is exposed to saturated DNT vapor in air at room temperature for 16 h the change in the properties of the polymer become so large that not only is the resonance wavelength shifted, but the shape of the resonance is also greatly altered and distorted. Since both microring resonators and fiber Bragg gratings are high Q optical resonators, the microring resonators sensors and fiber Bragg grating sensors should have comparable sensitivity and response time if the sensor film of the same polymer and same thickness is used.

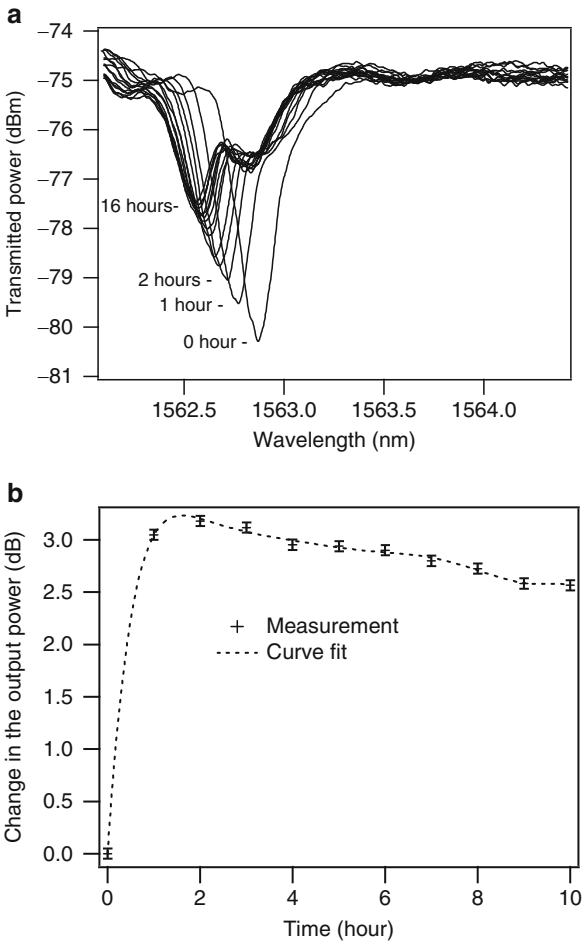

Fig. 2.15 (**a**) The change in the transmission spectrum of a fiber Bragg grating coated with DH6/PMMA in response to DNT. The sensor was exposed to saturated DNT vapor at room temperature. The measurements were taken at time intervals of one hour. The last measurement was taken after the sensor was exposed to DNT for 16 h. (**b**) The change of optical power at the output end of the fiber sensor for light of the wavelength of 1,562.9 nm. Reprinted from Ref. 33 with permission. © 2008 American Chemical Society

2.7 All-Dielectric Radio Frequency Electric Field Sensor

Optical sensors to measure electric field based on EO effect are useful for characterizing and testing high speed electronic devices and integrated circuits, electromagnetic compatibility measurements, electromagnetic imaging with millimeter and/or terahertz wave and radio frequency photonic links[39,40]. A number of optical electric field sensors based on Mach-Zehnder interferometers and polarization

modulation have been previously reported[41,42]. Microring resonators of high Q factor could enable higher sensitivity with a compact device size. EO polymers have high EO coefficients, low dielectric constants, and femtosecond time scale EO responses. They have good potential for optical electric field sensors with higher sensitivity, lower invasiveness, and higher bandwidth.

A novel radio-frequency electric field sensor based on an EO polymer microring resonator directly coupled to the core of a side-polished optical fiber, shown in Fig. 2.16, has been successfully demonstrated[14]. A cross-linkable EO polymer that contains AJLS102 chromophore[43] (Fig. 2.5) was used to make the microring resonator. A ~1.5 μm thin film was spin cast on a glass substrate coated with 100 nm of transparent conductive indium tin oxide (ITO). The film was subsequently electrically poled and cross-linked. The ITO was used as a poling electrode. The poled polymer film was then patterned with electron beam lithography and RIE. The patterned racetrack-shaped ring resonators had two semicircular sections of 35 μm radius and two straight sections of 50 μm in length. The waveguide width was 10 μm for better coupling with the fiber core. The transmission spectrum of the fiber was monitored while the EO polymer microring was being aligned to the fiber core at the polished region. After the best resonance extinction was reached the glass substrate of the ring was permanently attached to the fiber using a UV curable epoxy.

At a wavelength tuned at the slope of a resonance dip in the transmission spectrum, the intensity of the output light is modulated by the external radio frequency electric field. The variation of the output light intensity is proportional to the sharpness of the resonance, the intensity of the input light, and the strength of the electric field. The device showed a minimum detectable electric field intensity of 100 mV/m. This sensitivity was limited by the Q-factor of the resonator and the EO coefficient r_{33} of the EO polymer and the noise of the measurement system. The Q of the sensor is approximately 1,100, and therefore the theoretical bandwidth of the sensor is above 100 GHz. The device was tested at frequencies up to 550 MHz (Fig. 2.17), which is the upper limit of out test equipment. The Q is mostly limited by the absorption loss from ITO. EO polymer microring resonators without the ITO have demonstrated a Q-factor on the order of 10^5 [1], which translates to a sensitivity below 1 mV/m and bandwidth of 2 GHz. The excess loss of the fiber is on the order of 1 dB, due mostly to the roughness of the side-polish. Using the optical fiber itself as the bus waveguide and substrate avoids loss, reliability, and cost issues associated with the fiber-to-waveguide end coupling. It also eliminates high propagation loss coming from the long EO polymer waveguides in Mach-Zehnder type sensors. This structure allows the position of the ring to be adjusted to achieve optimal coupling and good resonance. The microring resonator can be either located in the middle of the fiber and operated in transmission configuration, or near one cleaved end of the fiber with a dielectric mirror coated on the end face and operate in reflection configuration like a needle-shaped EO probe. Using two-photon polymerization, it is also possible to make multiple rings directly on the side-polished flat surface of a free-standing fiber to form a sensor array, as shown in Fig. 2.16c.

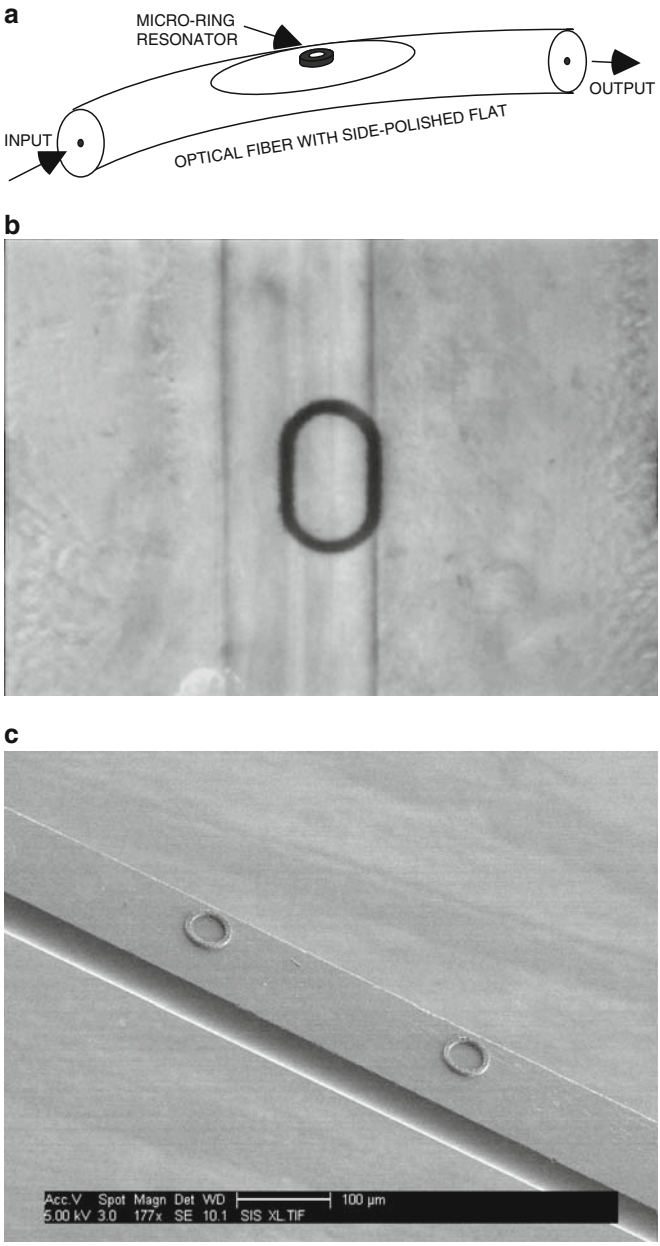

Fig. 2.16 (**a**) A schematic drawing of polymer microring resonator couple to a side-polished optical fiber. (**b**) A microscope image of the fabricated EO polymer electric field sensor. (**c**) SEM image of resonators fabricated on the polished flat of a free-standing fiber. The scale bar in the picture represents 100 µm. Reprinted from Ref. 15 with permission.

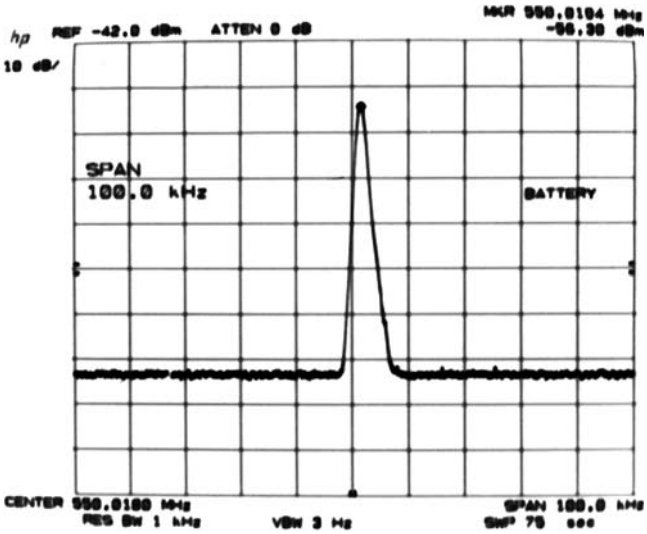

Fig. 2.17 The output of the RF electric field sensor at 550 MHz and 10 dBm RF input. Reprinted from Ref. 15 with permission. © 2008 Institute of Electrical and Electronics Engineers

2.8 Conclusion

Chromophore-doped polymers have great potential for many sensor applications. Key technologies of the design, fabrication, and electronic-photonic integration of polymer microring resonators and a number of novel microresonator sensors have been successfully developed. High Q factor of polymer microring resonators can be achieved through systematic design and optimization with fast BPM simulations and transfer matrix analysis. Chromophore-doped polymers also allow optical waveguides and microring resonators to be patterned using UV light and electron-beam in a single process step. Both methods are free of solvents, wet chemicals, and toxic gases. Microring resonators made with chromophore-doped polymer can be used to detect trace explosives. Detection sensitivity of DNT at ppb level with good specificity has been demonstrated, and the polymer has the potential of pushing the detection limit to the ppt level. An optical electric field sensor with an EO polymer microring coupled with a side-polished fiber was shown to have adequate sensitivity for many practical applications. This device structure uses a low loss optical fiber as a bus waveguide and greatly reduces the insertion loss from fiber-waveguide coupling and long EO polymer waveguides. Chromophores are man-made materials and as molecular design and organic synthesis continue to advance, new polymers with more desirable sensing properties will continue to emerge, enabling better sensors and new applications.

Acknowledgments The author thanks Profs. Larry R. Dalton and Alex K.-Y. Jen, and Lumera Corporation for providing polymer materials. The work present in this chapter is supported by

National Science Foundation Grant Number ECS-0437920, National Science Foundation Center on Materials and Devices for Information Technology Research (STC-CMDITR), Grant Number DMR-0120967, and Office of Naval Research Grant N00014–05–1–0843.

References

1 Rabiei, P.; Steier, W. H.; Zhang, Z.; Dalton, L. R., Polymer micro-ring filters and modulators, *J. Lightw. Technol.* **2002**, 20, 1968–1975
2 Dalton, L. R.; Robinson, B. H.; Jen, A. K.-Y.; Steier, W. H.; Nielsen, R., Systematic development of high bandwidth, low drive voltage organic electro-optic devices and their applications, *Opt. Mater.* **2003**, 21, 19–28
3 Enami, Y.; Peyghambarian, N.; Kawazu, M.; Jen, A. K. -Y., Hybrid electro-optic polymer and selectively buried sol-gel waveguides, *Appl. Phys. Lett.* **2003**, 82, 490–492
4 Sinyukov, A. M.; Hayden, L. M., Generation and detection of terahertz radiation with multilayered electro-optic polymer films, *Opt. Lett.* **2002**, 27, 55–57
5 Pyayt, A.; Zhang, X.; Luo, J.; Jen, A.; Dalton, L.; Chen, A., Optical micro-resonator chemical sensor, *Proc. SPIE* **2007**, 6556, 65561D-1–65561D-6
6 Little, B. E.; Chu, S. T.; Absil, P. P.; Hryniewicz, J. V.; Seiferth, F. G. F.; Gill, D.; Van, V.; King, O.; Trakalo, M., Very high-order microring resonator filters the WDM applications, *IEEE Photonics Technol. Lett.* **2004**, 16, 2263–2265
7 Xia, F.; Sekaric, L.; Vlasov, Y., Ultracompact optical buffers on a silicon chip, *Nat. Photonics* **2007**, 1, 65–71
8 Xu, Q.; Schmidt, B.; Pradhan, S.; Lipson, M., Micrometre-scale silicon electro-optic modulator, *Nature* **2005**, 435, 325–327
9 Dekker, R.; Klunder, D. J. W.; Borreman, A.; Diemeer, M. B. J.; Worhoff, K.; Driessen, A.; Stouwdam, J. W.; Van Veggel, F. C. J. M., Stimulated emission and optical gain in LaF_3:Nd nanoparticle-doped polymer-based waveguides, *Appl. Phys. Lett.* **2004**, 85, 6104–6106
10 Kuwata-Gonokami, M.; Jordan, R. H.; Dodabalapur, A.; Katz, H. E.; Schilling, M. L.; Slusher, R. E.; Ozawa, S., Polymer microdisk and microring lasers, *Opt. Lett.* **1995**, 20, 2093–2095
11 Chao, C. -Y.; Fung, W.; Guo, L. J., Polymer microring resonators for biochemical sensing applications, *IEEE J. Sel. Topics Quant. Electron.* **2006**, 12, 134–146
12 Steier, W. H.; Kalluri, S.; Chen, A.; Garner, S.; Chuyanov, V.; Ziari, M.; Shi, Y.; Fetterman, H.; Jalali, B.; Wang, W.; Chen, D.; Dalton, L. R., Applications of electro-optic polymers in photonics, *Mater. Res. Soc. Symp. Proc.* **1996**, 413, 147–157
13 Herminghaus, S.; Smith, B. A.; Swalen, J. D., Electro-optic coefficients in electric-field-poled polymer waveguides, *J. Opt. Soc. Am. B* **1991**, 8, 2311–2317
14 Sun, H.; Pyajt, A.; Luo, J.; Shi, Z.; Hau, S.; Jen, A. K. -Y.; Dalton, L.; Chen, A., All-dielectric electrooptic sensor based on a polymer microresonator coupled side-polished optical fiber, *IEEE Sens. J.* **2007**, 7, 515–524
15 Chen, A.; Sun, H.; Pyayt, A.; Dalton, L. R.; Luo, J.; Jen, A. K.-Y., Microring resonators made in poled and unpoled chromophore-containing polymers for optical communication and sensors, *IEEE J. Sel. Topics Quantum Electron.* **2008**, 14, 1281–1288
16 Homola, J.; Yee, S. S.; Gauglitz, G., Surface plasmon resonance sensors: review, *Sens. Actuators B* **1999**, 54, 3–15
17 Trouillet, A.; Ronot-Trioli, C.; Veillas, C.; Gagnaire, H., Chemical sensing by surface plasmon resonance in a multimode optical fibre, *Pure Appl. Opt.* **1996**, 5, 227–237
18 Ronot-Trioli, C.; Trouillet, A.; Veillas, C.; Gagnaire, H., Monochromatic excitation of surface plasmon resonance in an optical-fibre refractive-index sensor, *Sens. Actuators A* **1996**, 54, 589–593

19 Yariv, A., Universal relations for coupling of optical power between microresonators and dielectric waveguides, *Electron. Lett.* **2000**, 36, 321–322
20 Norwood, R. A.; Eldada, L.; Emo, S.; Gustus, J.; Rapoport, R.; Stengel, K. M. T.; Shacklette, L. W.; Wu, C.; Xu, C.; Yardley, J. T., Polymer optical interconnection technology: toward WDM applications, *Proc. SPIE* **1996**, 2690, 151–162
21 Eldada, L.; Xu, C.; Stengel, K. M. T.; Shacklette, L. W.; Yardley, J. T., Laser-fabricated low-loss single-mode raised-rib waveguiding devices in polymers, *J. Lightwave Technol.* **1996**, 14, 1704–1713
22 Eldada L.; Shacklette, L. W., Advances in polymer integrated optics, *IEEE J. Sel. Topics Quant. Electron.* **2000**, 6, 54–68
23 Wang, W. C.; Lin, W.; Marshall, H.; Skolnick, R.; Schaafsma, D., All-dielectric miniature wideband rf receive antenna, *Opt. Eng.* **2004**, 43, 673–677
24 Sun, H.; Dalton, L.; Chen, A., Systematic design and simulation of polymer microring resonators with the combination of beam propagation method and matrix model, In Digest of the IEEE LEOS Summer Topical Meetings, 2007, 217–218
25 Paloczi, G. T.; Huang, Y.; Yariv, A.; Mookherjea, S., Polymeric Mach-Zehnder interferometer using serially coupled microring resonators, *Opt. Express* **2003**, 11, 2666–2671
26 Ma, J.; Lin, S.; Feng, W.; Feuerstein, R. J.; Hooker, B.; Mickelson, A. R., Modeling photo-bleached optical polymer waveguides, *Appl. Opt.* **1995**, 34, 5352–5360
27 Chen, A.; Chuyanov, V.; Marti-Carrera, F. I.; Garner, S.; Steier, W. H.; Mao, S. S. H.; Ra, Y.; Dalton, L. R.; Shi, Y., Trimming of polymer waveguide Y-junction by rapid photobleaching for tuning the power splitting ratio, *Photonics Technol. Lett.* **1997**, 9, 1499–1501
28 Zhou, J.; Pyayt, A.; Dalton, L. R.; Luo, J.; Jen, A. K. Y.; Chen A., Photobleaching fabrication of microring resonator in a chromophore-containing polymer, *IEEE Photonics Technol. Lett.* **2006**, 18, 2221–2223
29 Liao, Y.; Anderson, C. Y.; Sullivan, P. A.; Akelaitis, A. J. P.; Robinson, B. H.; Dalton, L. R., Electro-optical properties of polymers containing alternating nonlinear optical chromophores and bulky spacers, *Chem. Mater.* **2006**, 18, 1062–1067
30 Jin, D.; Londergan, T.; Huang, D.; Wolf, N.; Condon, S.; Tolstedt, D.; Guan, H. W.; Cong, S.; Johnson, E.; Dinu, R., Achieving large electro-optic response: DH-type chromophores in both crosslinked systems and linear high-Tg systems, *Proc. SPIE* **2004**, 5351, 44–56
31 Luo, J.; Liu, S.; Haller, M.; Kang, J. -W.; Kim, T. -D.; Jang, S. -H.; Chen, B.; Tucker, N.; Li, H.; Tang, H. -Z.; Dalton, L. R.; Liao,Y.; Robinson, B. H.; Jen A. K. Y., Recent progress in developing highly efficient and thermally stable nonlinear optical polymers for electro-optics, *Proc. SPIE* **2004**, 5351, 36–43
32 Samoc, A.; Samoc, M.; Luther-Davies, B.; Kolev, V. Z.; Bagien, R. K.; Luo, X.; Zha, C., In situ second harmonic generation in disperse red 1 doped polymer and sol-gel films, *Molecular Cryst. Liq. Cryst.* **2006**, 446, 123–140
33 Chen, A.; Sun, H.; Pyayt, A.; Zhang, X.; Luo, J.; Jen, A.; Sullivan, P. A.; Elangovan, S.; Dalton, L. R.; Dinu, R.; Jin, D.; Huang, D., Chromophore-containing polymers for trace explosive sensors, *J. Phys. Chem. C* **2008**, 112, 8072–8078
34 Jose, A.; Zhu, Z.; Madigan, C. F.; Swager, T. M.; Bulovic, V., Sensitivity gains in chemosensing by lasing action in organic polymers, *Nature* **2005**, 434, 876–879
35 Bauer, W. S.; Yilmaz, S.; Wirges, W.; Gerhard-Multhaupt, R., Optimized poling of nonlinear optical polymers based on dipole-orientation and dipole-relaxation studies, *J. Appl. Phys.* **1994**, 75, 7211–7219
36 Hill, R. A.; Knoesen, A.; Mortazavi, M. A., Corona poling of nonlinear polymer thin films for electro-optic modulators, *Appl. Phys. Lett.* **1994**, 65, 1733–1735
37 Vorst, C. P. J. M. V. D.; Picken, S. J., Electric field poling of acceptor-donor molecules, *J. Opt. Soc. Am B* **1990**, 7, 320–325.
38 Dalton, L. R.; Robinson, B. H.; Jen, A.-K. Y.; Reid, P.; Eichinger, B.; Sullivan, P.; Akelaitis, A.; Bale, D.; Haller, M.; Luo, J.; Liu, S.; Liao, Y.; Firestone, K.; Bhatambrekar, N.; Bhattacharjee, S.; Sinncss, J.; Hammond, S.; Buker, N.; Snoeberger, R.;

Lingwood, M.; Rommel, H.; Amend, J.; Jang, S. H.; Chen, A.; Steier, W., Electro-optic coefficient of 500 pm/V and beyond for organic materials, *Proc. SPIE* **2005**, 5935, 1–12
39 Robertson, W. M. Optoelectronic Techniques for Microwave and Millimeter-Wave Engineering, Artech House, Norwood, MA, 1995
40 Ozaki, K.; Sekiguchi, H.; Wakana, S.; Goto, Y.; Umehara, Y.; Matsumoto, J., Novel optical probing system with submicron spatial resolution for internal diagnosis of VLSI circuits, *Proc. Int. Test. Conf.* **1996**, 269–275
41 Zhang, F.; Chen, F.; Qiu, K., An integrated electro-optic E-field sensor with segmented electrodes, *Microw. Opt. Tech. Lett.* **2004**, 40, 302–305
42 Yang, K.; Katehi, L. P. B.; Whitaker, J. F., Electric field mapping system using an optical-fiber-based electrooptic probe, *IEEE Microw. Wireless Comp. Lett.* **2001**, 11, 164–166
43 Shi, Z.; Hau, S.; Luo, J.; Kim, T.-D.; Tucker, N. M.; Ka, J.-W.; Sun, H.; Pyajt, A.; Dalton, L.; Chen, A.; Jen, A. K.-Y., Highly efficient diels-alder crosslinkable electro-optic dendrimers for electric-field sensors, *Adv. Funct. Mater.* **2007**, 17, 2557–2563

http://www.springer.com/978-0-387-98060-7

Advanced Photonic Structures for Biological and Chemical Detection

Fan, X. (Ed.)
2009, XX, 540 p., Hardcover
ISBN: 978-0-387-98060-7